Astronomy & Astrophysics manuscript no. output
December 21, 2023

Calibration of Binary Population Synthesis Models Using A Sample of White Dwarf Binaries from APOGEE/Galex/Gaia

A. C. Rubio[1, 2]
C. Badenes[3], K. Breivik[4]

[1] Instituto de Astronomia, Geofísica e Ciências Atmosféricas, Universidade de São Paulo, Rua do Matão 1226, Cidade Universitária, 05508-900 São Paulo, SP, Brazil
[2] European Organisation for Astronomical Research in the Southern Hemisphere (ESO), Karl-Schwarzschild-Str. 2, 85748 Garching b. München, Germany
e-mail: amanda.rubio@usp.br
[3] Department of Physics and Astronomy and Pittsburgh Particle Physics, Astrophysics and Cosmology Center (PITT PACC), University of Pittsburgh, 3941 O'Hara Street, Pittsburgh, PA 15260, USA
[4] Department of Physics, McWilliams Center for Cosmology and Astrophysics, Carnegie Mellon University, 5000 Forbes Avenue, Pittsburgh, PA 15213, USA

Received September 15, 1996; accepted March 16, 1997

ABSTRACT

1. The population of White Dwarf binaries

White dwarfs (WD) are the final stage of evolution for the majority of stars, and as such provide useful information for studies of stellar populations. While they are a straightforward end-point for low mass single stars, WDs can also be formed via binary evolution and even be the result of mergers.

A binary system containing a WD can be formed through many evolutionary channels (Fig. 2). Two stars can be born in a binary system but be separated enough to never interact; as they evolve as single stars, the result can be a WD and a Main Sequence (MS), giant, or another WD, depending mostly on their initial mass ratio. If the two stars are born close enough to interact, a WD can also be formed after a period of mass transfer, which can be stable or unstable. In stable mass transfer, the would-be WD evolves out of the MS and fills its Roche lobe, donating mass to its companion. Depending on the stage of evolution of the two stars and their separation, this mass transfer can become unstable, leading to a common envelope (CE) phase. Once again, this evolution can result in a WD binary (Toonen et al. 2017).

Whether the system goes through stable or unstable mass transfer, the imprints of its evolution are left on the parameters of the final systems, such as on their periods. While these signs are not unambiguous, they provide important clues to our understanding of binary evolution, in particular on the still poorly understood CE phase. Zorotovic et al. (2010), for instance, uses a sample of WD+MS binaries from SDSS to estimate the efficiency of envelope ejection after the CE phase, α, finding values in range of $0.2 - 0.3$ to represent the final parameters of most of their sample. The recent work of Scherbak & Fuller (2023) models the CE phase of 10 WD binary systems using stellar evolution code MESA, finding a similar range for α, $0.2 - 0.4$.

In this work, we aim to calibrate the mass transfer parameters of binary population synthesis (BPS) models of the code COSMIC (Breivik et al. 2020) with a sample of WD binaries from the APOGEE-Galex-Gaia catalog (Anguiano et al. 2022). We explore in our COSMIC models different α, limits on the accretion during RLO, and criteria for on the onset of unstable mass transfer. These models are compared to the data of WD+MS systems by their $\Delta RV_{\rm max}$, a proxy for period. The data is described in Sect. 2, COSMIC and the models we calculated in Sect. 3, our preliminary results are in Sect. 4, and the next steps of this project in Sect. 5.

2. APOGEE-Gaia-Galex catalog (AGGC)

AGGC is a catalog of candidate binaries containing WD stars. It was compiled by (Anguiano et al. 2022) using near-infrared data from the Apache Point Observatory Galactic Evolution Experiment (APOGEE - data release 17) project (Majewski et al. 2017), UV data from GALEX (Bianchi et al. 2017), and optical data from the Gaia mission (Lindegren et al. 2021). With this combination, AGGC was able to identify WDs in systems with stars in a broad range of luminosities, from low mass MS stars to giants.

Fig. 1 gives an overview of the data, focusing on the WD+MS binaries we are interested in this work. In the upper left panel, we show the HR diagram for the entire APOGEE sample, with the WD binaries of all classes highlighted. The black lines define three regions: the red giant branch (RGB), and the MS ($log\, g < 4$), further divided into hot ($T_{\rm eff} > 5500K$) and cold ($T_{\rm eff} < 5500K$). In total, AGGC contains 588 WD+MS systems: 428 in the cold MS and 187 in the hot MS.

In the upper right panel of Fig. 1, we compare the distribution of the maximum and minimum values of radial velocity measurements, $\Delta RV_{\rm max}$, between subsets of the AGCC sample, particularly for WD+MS binaries. Out of the many parameters AGGC has of its WD binary systems, $\Delta RV_{\rm max}$ has a direct connection to the period of the system. The largest RV shifts will happen for systems where the gravitational forces of the two stars affect each other more strongly, which happens for tighter systems, with smaller periods; in systems with larger periods, the orbital velocities of the stars are lower, and thus $\Delta RV_{\rm max}$ is also smaller. Thus, $\Delta RV_{\rm max}$ is a valuable proxy for period, as

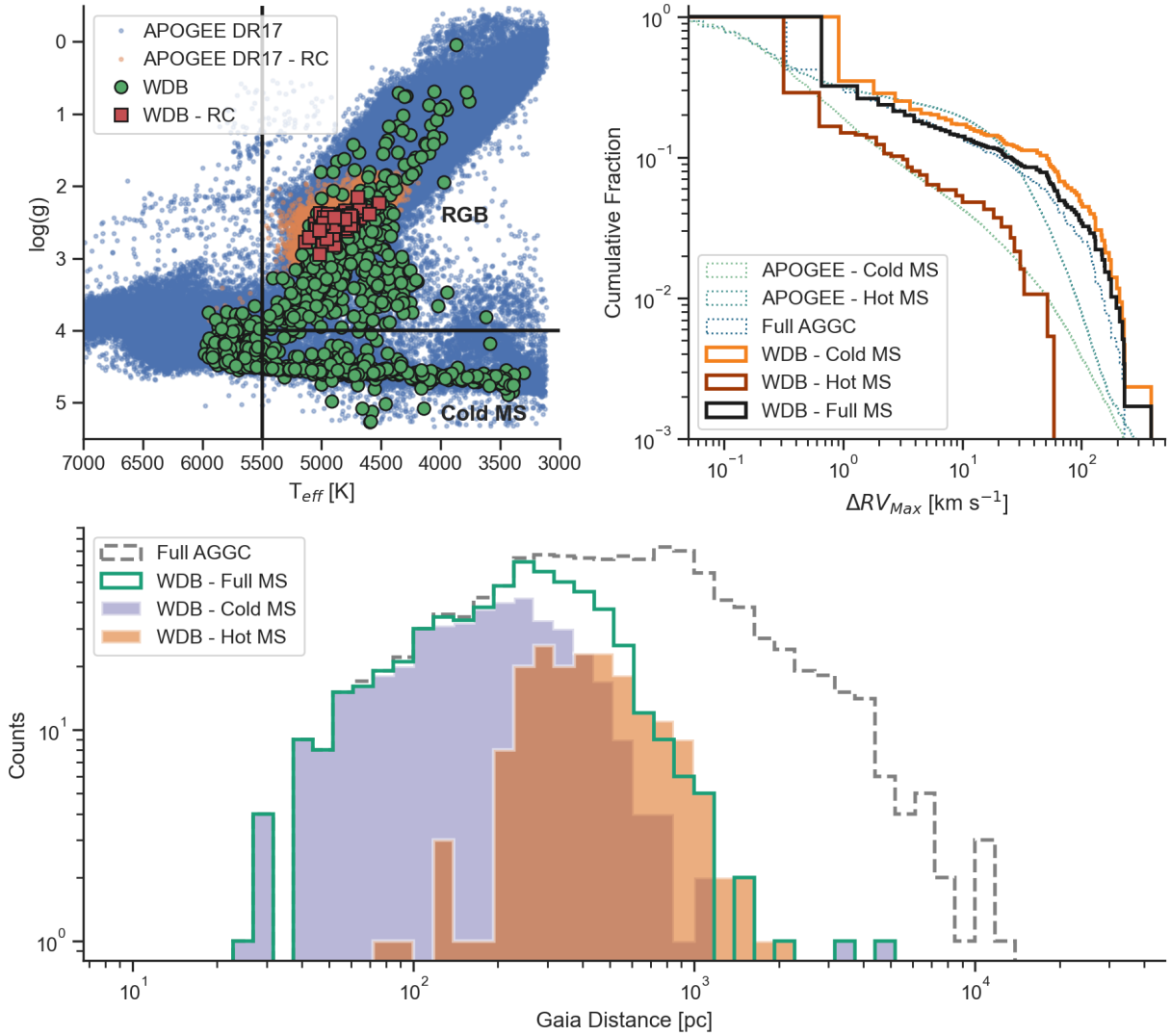

Fig. 1. Overview of the white dwarf binaries in the APOGEE-Gaia-Galex catalog. Upper left panel shows the full APOGEE DR17 data in blue, APOGEE data of red clump stars in orange, and the companions of WDs in green and red, for the red clump. Upper left panel shows the $\Delta RV_{\rm max}$ distribution for different cuts in the data: hot and cold MS from the full APOGEE DR17, all WD binaries in AGGC, in blue tones, doted lines, and WD with hot and cold MS companions in orange, red and black, full lines. The lower panel shows the Gaia distance of the systems, for the full AGGC, and for WD binaries with hot and cold MS companions.

finding the periods of binary systems requires long term monitoring, while $\Delta RV_{\rm max}$ can be determined with only a few measurements. The shape of the cumulative distribution of $\Delta RV_{\rm max}$ for the WD+MS binaries of both the hot and cold MS has a notably different shape than the distribution for the full APOGEE DR17 for MS stars, skewing to larger $\Delta RV_{\rm max}$ values, which indicates WD+MS systems tend to have shorter periods. Finally, the lower panel of Fig. 1 shows the distance distribution for the AGGC data, with a higher number of cold MS stars being visible at smaller distances. Excluding the more evolved and bright RGB stars as companions, the distances covered by the sample are closer.

3. Binary population synthesis with COSMIC

Binary population synthesis (BPS) codes are widely used in the study of populations of single and binary stellar populations. As BPS are based on simplified prescriptions for the key evolutionary processes of the system, such as mass transfer, they are much faster than stellar evolution codes which evolve the stellar structure equations in real time. Thus, great numbers of systems can be simulated in a time-efficient manner, and the qualitative trends in the population can be analyzed.

In this work, we use the BPS code COSMIC (Breivik et al. 2020). We created a grid of COSMIC populations, each containing 10000 binaries. As COSMIC has dozens of input parameters, we kept most of them fixed; all our populations are initialized with the initial mass function (IMF) from Kroupa (2001), an uniform eccentricity distribution, and the period distribution from Raghavan et al. (2010). The populations all have solar metallicity and a uniform star formation history over the last 10 Gyr.

COSMIC has several parameters that control the evolution of its binaries. Our main interest in this work are binary systems where one of the members is a white dwarf and the other a MS star. From theory, these WD+MS systems can form via many evolutionary channels, and binary interaction is not a necessity (see Fig. 2). As COSMIC simulates thousands of systems, our sample will contain WD+MS binaries that evolved differently: some will have undergone only stable mass transfer, some will have undergone common envelope, and some will have not in-

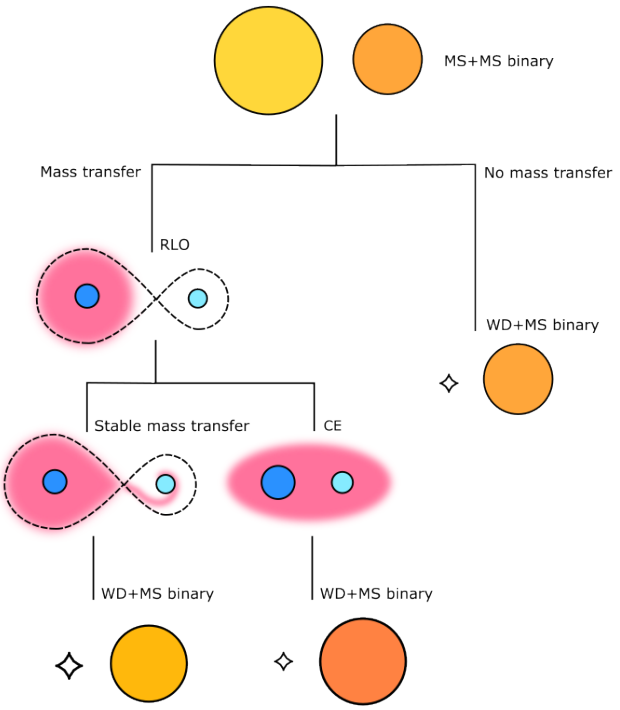

Fig. 2. Schematic of the possible evolutionary paths a binary system can go through to become a WD+MS binary. The system can either not interact, or go through mass transfer, which can in turn be stable (Roche lobe overflow) or unstable, leading to a common envelope phase.

teracted at all, with the WD formed via single stellar evolution. Changing the parameters of COSMIC changes the recipes of the interactions these systems go through, thus significantly modifying the evolution and final characteristics of the simulated WD+MS population.

We explore three key binary evolution parameters in our COSMIC grid:

- $\mathrm{acc_{lim}}$, which limits the amount of mass accreted during Roche-lobe overflow. This parameter sets overall fraction of donor material that is accreted, with the rest being lost from the system ($\mathrm{acc_{lim}}$ = 0.5 assumes 50% accretion efficiency) (Belczynski et al. 2008). Values range from 0 to 1.
- α, the common envelope efficiency parameter, which scales the efficiency of transferring orbital energy to the envelope to eject it, as $E_{\mathrm{bind,i}} = \alpha(E_{\mathrm{orb,f}} - E_{\mathrm{orb,i}})$, Eq. 71 of Hurley et al. 2002. An α = 1 indicates that all of the orbital energy of the system was used to unbind the envelope; larger values assume all of the orbital energy and energy from another, unspecified source, were used.
- $\mathrm{qc_{flag}}$, which selects the model used to determine critical mass ratios for the onset of unstable mass transfer and/or a common envelope during RLO. There are six available prescriptions in COSMIC:
  - $\mathrm{qc_{flag}}$ = 0: Hurley et al. (2002) (standard BSE);
  - $\mathrm{qc_{flag}}$ = 1: Hurley et al. (2002) with Hjellming & Webbink (1987)'s treatment for giant and asymptotic giant branch (GB and AGB) stars;
  - $\mathrm{qc_{flag}}$ = 2: Claeys et al. (2014);
  - $\mathrm{qc_{flag}}$ = 3: Claeys et al. (2014) with Hjellming & Webbink (1987)'s treatment GB/AGB stars;
  - $\mathrm{qc_{flag}}$ = 4: Belczynski et al. (2008), except for WD donors which follow BSE;
  - $\mathrm{qc_{flag}}$ = 5: Neijssel et al. (2019).

$$q_c = 0.362 + \left[3.0\left(1.0 - \frac{M_{c1}}{M_1}\right)\right]^{-1} \quad (1)$$

$$q_c = 2.13\left[1.67 - x + 2\left(\frac{M_{c1}}{M_1}\right)^5\right]^{-1} \quad (2)$$

We created 27 models varying these three parameters according to Table 2. The models can be separated in 8 categories: models in families A, B and C have the same α, but vary $\mathrm{acc_{lim}}$ (letters) and $\mathrm{qc_{flag}}$ (1 to 4); models D, E, F, G and H vary α (letters) and $\mathrm{acc_{lim}}$ (0, 0.5 and 1), but keep $\mathrm{qc_{flag}}$ fixed. Fig. 3 shows the variation in the orbital period of the WD+MS binaries in each of the models, colored by the type of interaction the system went through during its evolution. The majority of systems, for all models, become a WD+MS system without ever interacting (blue boxes); these systems have the largest periods, as it is necessary that they be wider to avoid interaction in the first place, and remain wide until one of the stars become a WD. In all models, T the systems with the shortest periods are the ones that undergo common envelope evolution. To go through CE in the first place, the two stars must already be close at birth; the transfer of mass and AM as they evolve makes the system tighter throughout their lifetime. Many of these systems merge, and the ones that survive CE phase end up as binaries with very short periods.

Whether a system goes through only stable mass transfer (RLO) or also through a phase of unstable mass transfer (such as CE) depends not only on the initial separation of the system, but also on the amount of mass accreted during Roche-lobe overflow ($\mathrm{acc_{lim}}$), and the critical value for the mass ratio between the core and envelope of the donor star ($\mathrm{q_{crit}}$). This critical value in turn depends on its evolutionary state, following Table 1. In model families A, B and C, we explore four prescriptions for $\mathrm{qc_{flag}}$. As shown in Fig. 3 (upper three panels), the relative number of systems that go through no mass transfer, only RLO, and CE vary little between $\mathrm{qc_{flag}}$ = 1 and 3, with more significant, but still relatively small, changes for $\mathrm{qc_{flag}}$ = 2. For $\mathrm{qc_{flag}}$ = 4, however, there is a larger number of systems that go only through stable mass transfer for all the explored values of $\mathrm{acc_{lim}}$, due to the larger values set for the onset of unstable mass transfer. For model families D, E, F, G and, H, where we explore α and $\mathrm{acc_{lim}}$ (Fig. 3, lower five panels), we see that $\mathrm{acc_{lim}}$ has a much more significant effect on the number of systems that go stable or unstable mass transfer, and on the resulting orbital period of these systems. Models with full conservative accretion ($\mathrm{acc_{lim}}$ = 1) form binaries with periods of around 1000 days via RLO, but slide more easily into CE as the conservation of angular momentum shrinks the orbit of system more effectively than in the models with non-conservative mass transfer.

Fig. 4 shows the histograms of the period distribution of the models for the systems that undergo some sort of mass transfer. There is a gap in the period distribution of the models from about 200-1000 days in family models A, B, C, D and E, with the clear exception of the models with $\mathrm{qc_{flag}}$ = 4 (A4, B4 and C4). In these models (A4, B4, C4), as the threshold for unstable mass transfer is higher, the two stars can come closer together and remain in a stable mass transfer scenario; there is still a gap in the period distributions of these models, but it happens at around 10 days.

The gap is a consequence of the RLO phase (systems that go through CE are all in the shorter period range): bimodal distributions are present for nearly all models in Fig. 3. Although

Evolutionary state of donor	q_{crit} value			
	$qc_{flag} = 1$	$qc_{flag} = 2$	$qc_{flag} = 3$	$qc_{flag} = 4$
MS, < 0.7 $M_\odot$	0.695	0.695 / 1.0	0.695 / 1.0	3.0
MS, > 0.7 $M_\odot$	3	1.6 / 1.0	1.6 / 1.0	3.0
Hertzsprung Gap	4	4.0 / 4.7619	4.0 / 4.7619	3.0
First Giant Branch	Eq. 1	Eq. 2 / 1.15	Eq. 1 / 1.15	3.0
Core Helium Burning	3	3.0 / 3.0	3.0 / 3.0	3.0
Early Asymptotic Giant Branch (AGB)	Eq. 1	Eq. 2 / 1.15	Eq. 1 / 1.15	3.0
Thermally Pulsing AGB	Eq. 1	Eq. 2 / 1.15	Eq. 1 / 1.15	3.0
Naked Helium Star MS	3	3.0 / 3.0	3.0 / 3.0	1.7
Naked Helium Star Hertzsprung Gap	0.784	4.0 / 4.7619	4.0 / 4.7619	3.5
Naked Helium Star Giant Branch	0.784	0.784 / 1.15	0.784 / 1.15	3.5

Table 1. Values for q_{crit} according to the evolutionary state of the donor star for each qc_{flag}. Eq. 1 from Hjellming & Webbink (1987) and Eq. 2 from Claeys et al. (2014).

the bimodality and gap remain nearly constant between different model families, the distribution of the periods of systems that go through CE moves towards larger periods as α increases (black dashed lines in Fig. **??**). As the envelope ejection efficiency increases, less orbital energy is necessary to eject it, thus leading to systems with slightly larger separations, and therefore periods, blending away the gap in models F, G and H.

The cause of the gap is likely the boundary between stable and unstable mass transfer. The systems that cross this boundary, having the necessary conditions in mass, radius and separation, enter a common envelope phase, where mass and angular momentum transfer quickly tighten orbit the system.The differences in the size and exact position of the gap in period space depend, therefore, on the evolutionary parameters that control the stable/unstable boundary of mass transfer, which explains the drastic difference for models with $qc_{flag} = 4$ from the rest of the models.

Preliminary analysis of the data shows that it is possible a gap also exists in the period distribution of the WD+MS binaries in the AGGC data. The significance of the gap will be explored in more detail as this project develops, but this can in principle be used to further constrain the evolutionary parameters of our simulations.

4. Results and discussion

4.1. ΔRV_{max} distribution

In our COSMIC models, we have the periods of the simulated systems, as shown in Figs. 3 and 4. To compare the models to AGGC data, we created a ΔRV_{max} distributions based on their period distribution. The periods, mass ratios and eccentricities of the COSMIC models were given as input to a Monte Carlo code (Badenes et al. 2018) that also generated random inclinations and arguments of pericenter for these systems. With all the orbital information for the systems in hand, the MC code could find RV values for the COSMIC models for a given distribution of time lags (times at which these RV "measurements" were taken for each system). We used the time lags of APOGEE DR17. Finally, from the full RV distribution we could extract a ΔRV_{max} distribution. As this is a MC code, the distribution can be sampled many times, i. e., many values of RV can be obtained for the same system, given that its inclination, argument of pericenter and time lag change each time we run the code. Thus, we could also estimate the uncertainty of ΔRV_{max} distribution for our COSMIC models. For our comparison of data and models, we created 100 MC sampled ΔRV_{max} distributions for each of our 27 models.

Model name	α	acc_{lim}	qc_{flag}
A1	0.25	0	1
A2	0.25	0	2
A3	0.25	0	3
A4	0.25	0	4
B1	0.25	0.5	1
B2	0.25	0.5	2
B3	0.25	0.5	3
B4	0.25	0.5	4
C1	0.25	1	1
C2	0.25	1	2
C3	0.25	1	3
C4	0.25	1	4
D0	0.75	0	1
D0.5	0.75	0.5	1
D1	0.75	1	1
E0	1	0	1
E0.5	1	0.5	1
E1	1	1	1
F0	3	0	1
F0.5	3	0.5	1
F1	3	1	1
G0	5	0	1
G0.5	5	0.5	1
G1	5	1	1
H0	7	0	1
H0.5	7	0.5	1
H1	7	1	1

Table 2. Overview of the parameters and names of 27 COSMIC models used in this work. Models are referred to by their names throughout the text.

Fig. 5 shows the comparison between the ΔRV_{max} cumulative fraction of our 27 models with the data from AGCC for the WD+MS binaries. In model families A, B and C, which have α = 0.25 and acc_{lim} = 0, 0.5 and 1, respectively, the effect of the different qc_{flag} in each of models on the ΔRV_{max} distribution is

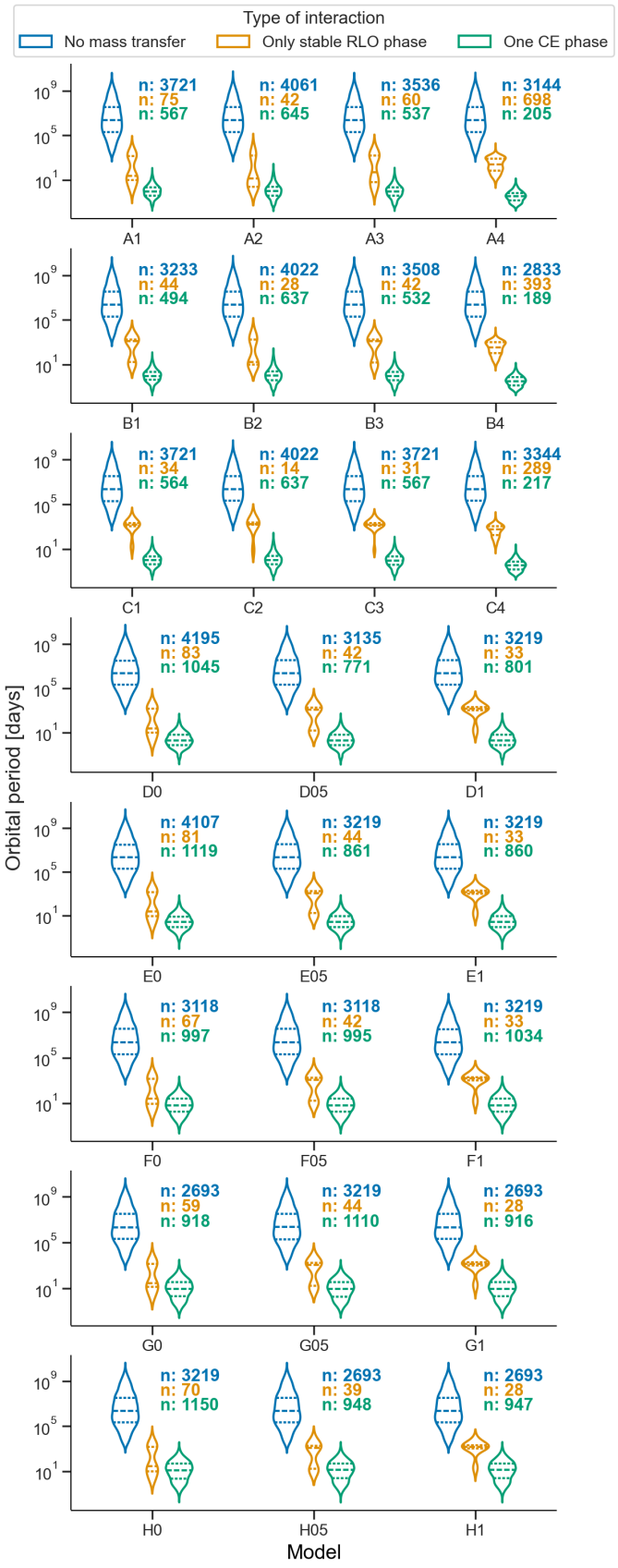

Fig. 3. Violin plots of the WD+MS binary systems in each of our 27 COSMIC models, colored according to the type of interaction the system went through during its evolution. The printed values indicate how many systems are in each category.

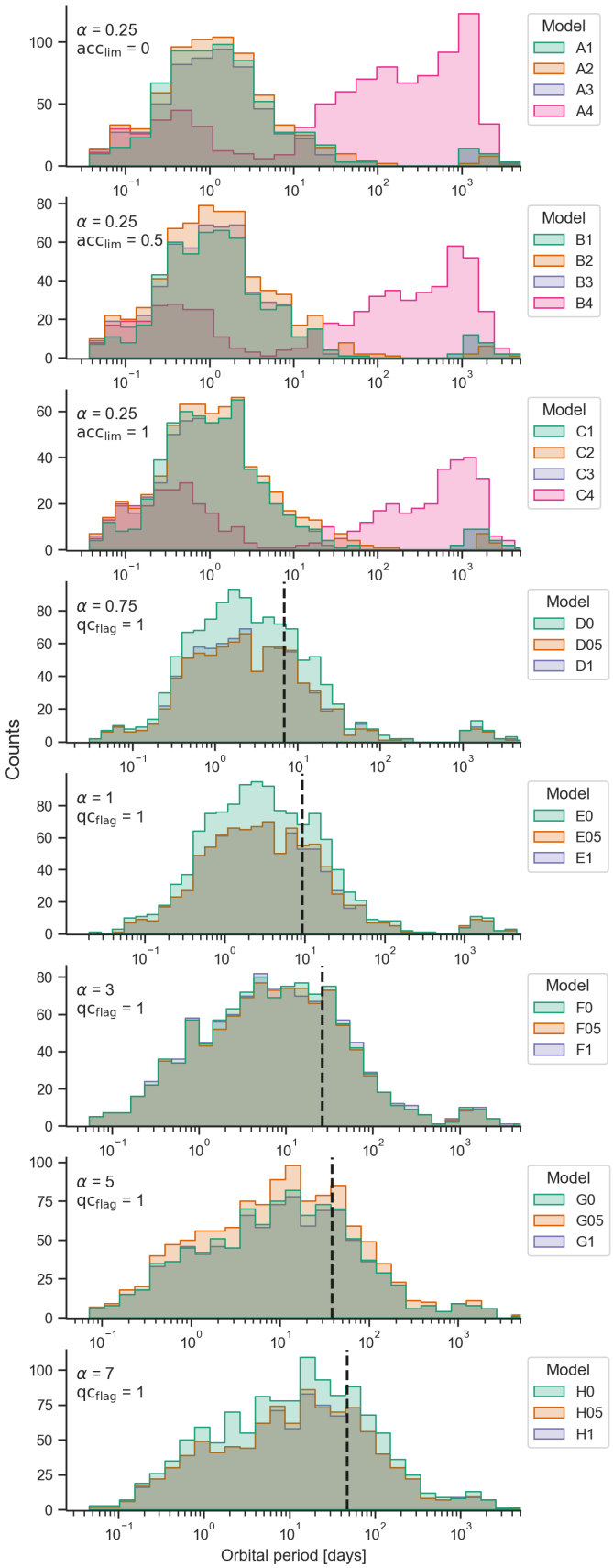

Fig. 4. Final period distribution of the WD+MS binaries that went through mass transfer, either stable or unstable. The dashed black lines in the lower panels represent the mean of the distribution of only the systems that went through a common envelope phase.

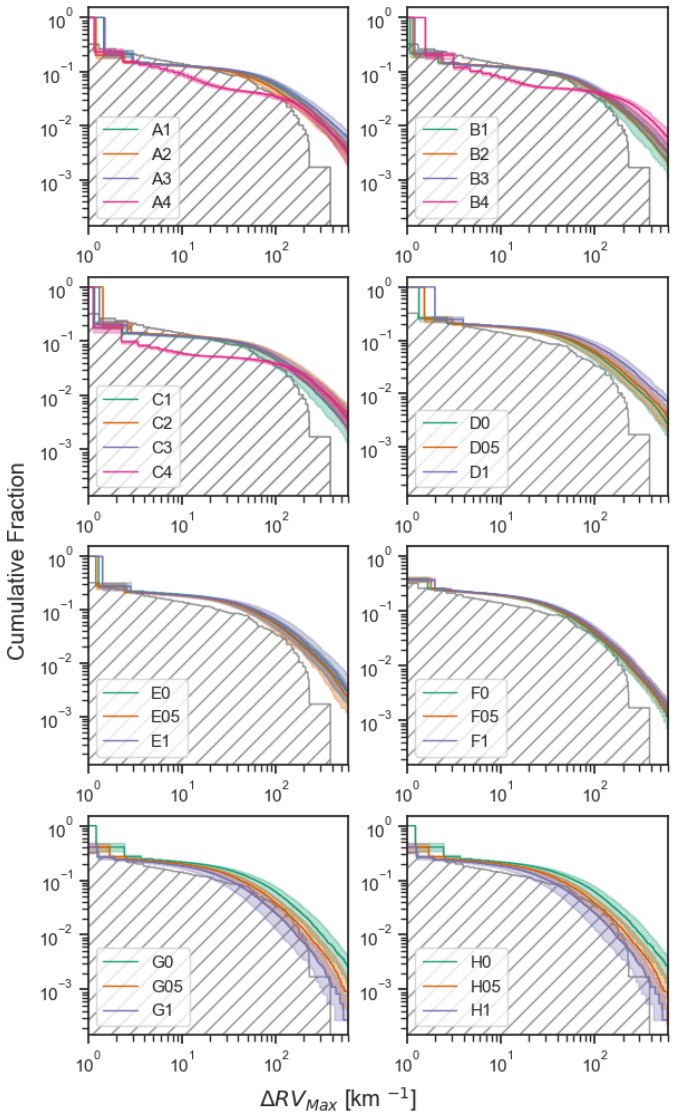

Fig. 5. Cumulative distributions for the $\Delta RV_{\rm max}$ of the models and AGCC sample of WD+MS binaries (in gray, hatched). The shaded colored regions represent the 15%-85% quartiles of the 100 MC simulations used to calculate the $\Delta RV_{\rm max}$ curve for for each COSMIC model.

significant. Models with $\rm qc_{flag} = 4$ particularly have difficulty in reproducing the data in lower and middle $\Delta RV_{\rm max}$ values, which represent the systems with larger orbital periods. The effect of $\rm acc_{lim}$ increases as with $\Delta RV_{\rm max}$, becoming more important at the tails of the distribution, particularly for models G and H. The parameter α is the main responsible for the curvature of the distribution: models with larger α have a steeper drop-off. In other words, models low α overestimate the amount of short period systems. From visual inspection alone, the models that come closer to reproducing the $\Delta RV_{\rm max}$ distribution of the data are G1 and H1.

To quantitatively compare the $\Delta RV_{\rm max}$ distributions of the AGGC data and of our COSMIC populations, we used the Kolmogorov-Smirnov (KS) and the Anderson-Darling (AD) statistical tests. The distributions were compared in the range $10 < \Delta RV_{\rm max} < 400\ km^{-1}$. We use all four tests on all 100 MC sampled $\Delta RV_{\rm max}$ values for each of the models. For all models in families A, B and C, the null-hypothesis that data and models were sampled from the same underlying distribution is rejected at a confidence level of 95% (or higher) for both the KS and AD test. For models with higher α, starting with models D, begin to show a better agreement between data and models. The null-hypothesis, for models D, G0 and H0, cannot be rejected with a significance above 10%, and 15% for models E, F, G0.5, G1, H0.5 and H1 in the AD test, and between 10 and 15% for all models in the KS test. Therefore, our results indicate that the AGGC data for WD+MS binaries is better reproduced by COSMIC models with larger values of common envelope efficiency parameter, α.

While the statistical tests favor models with higher α, the period gap discussed in Sect. 3 can provide another, opposite constrain if further analysis of the data confirms the gap is present, since, as shown in Fig. 4 models with higher α cannot reproduce it. Also playing against the higher α is the lack of explanation for the source of this extra energy necessary to eject the envelope, going as large as 7 times the binding energy of the system.

5. Next steps

We are excited to continue this project, which we believe will soon develop into a paper. Our immediate next steps are to confirm the period gap in the AGGC data, which would have important consequences for our conclusions. If indeed the data shows a gap, this information will have to be properly accounted for when comparing data and model $\Delta RV_{\rm max}$ distributions, perhaps as a prior, in which case we must rethink our statistical analysis as a whole.

Acknowledgements. This work was initiated at the Kavli Summer Program in Astrophysics 2023, hosted at the Max Planck Institute for Astrophysics. We thank the Kavli Foundation and the MPA for their support.

References

Anguiano, B., Majewski, S. R., Stassun, K. G., et al. 2022, AJ, 164, 126
Badenes, C., Mazzola, C., Thompson, T. A., et al. 2018, ApJ, 854, 147
Belczynski, K., Kalogera, V., Rasio, F. A., et al. 2008, ApJS, 174, 223
Bianchi, L., Shiao, B., & Thilker, D. 2017, The Astrophysical Journal Supplement Series, 230, 24
Breivik, K., Coughlin, S., Zevin, M., et al. 2020, ApJ, 898, 71
Claeys, J. S. W., Pols, O. R., Izzard, R. G., Vink, J., & Verbunt, F. W. M. 2014, A&A, 563, A83
Hjellming, M. S. & Webbink, R. F. 1987, ApJ, 318, 794
Hurley, J. R., Tout, C. A., & Pols, O. R. 2002, MNRAS, 329, 897
Kroupa, P. 2001, MNRAS, 322, 231
Lindegren, L., Klioner, S. A., Hernández, J., et al. 2021, A&A, 649, A2
Majewski, S. R., Schiavon, R. P., Frinchaboy, P. M., et al. 2017, AJ, 154, 94
Neijssel, C. J., Vigna-Gómez, A., Stevenson, S., et al. 2019, MNRAS, 490, 3740
Raghavan, D., McAlister, H. A., Henry, T. J., et al. 2010, ApJS, 190, 1
Scherbak, P. & Fuller, J. 2023, MNRAS, 518, 3966
Toonen, S., Hollands, M., Gänsicke, B. T., & Boekholt, T. 2017, A&A, 602, A16
Zorotovic, M., Schreiber, M. R., Gänsicke, B. T., & Nebot Gómez-Morán, A. 2010, A&A, 520, A86